Characterization of the Permittivity of Enameled Wires in Inverter-Driven Low-Voltage Electrical Machines

Niklas Driendl, Alaa Eddine Othman, Kay Hameyer
Institute of Electrical Machines (IEM)
RWTH Aachen University
Aachen, Germany
niklas.driendl@iem.rwth-aachen.de

2023 IEEE International Electric Machines & Drives Conference (IEMDC) | 979-8-3503-9899-1/23/$31.00 ©2023 IEEE | DOI: 10.1109/IEMDC55163.2023.10239078

***Abstract*—The use of inverters with high slew rates (du/dt) poses challenges to the insulation system of low-voltage electrical machines. Due to the fast-rising voltage pulses, a high overshoot at the terminals of the electric machine is expected. The electrical stress on the insulation system is determined by the electric field. Besides the applied voltage, the electric field is also depending on the permittivity of the insulation materials. If the critical electric field is exceeded, partial discharge can occur leading to premature failure of the machine. In the design process of the insulation system, the permittivity is usually considered as a constant value taken from data sheets or other literature. To predict the electric stress on the insulation appropriately, the permittivity has to be determined for the particular operation conditions. In this work, an approach to determine the permittivity at fast-rising bipolar voltage pulses is developed.**

***Index Terms*—electrical machine, insulation system, insulation material**

I. Introduction

The insulation system of inverter-driven electrical machines is focusing challenges due to current trends, particularly in automotive industry. On the one hand, the dc-link voltage is increasing to achieve a faster charging process of the battery of electric vehicles [1]. On the other hand, the use of fast-switching semiconductors [2] is aspired to reduce switching losses of the inverter. The fast-rising voltage edges cause overvoltages at the machine's terminals. Both effects lead to higher electric stress of the insulation system determined by the electric field between two conducting materials [3]. If the critical electric field inside the insulation system is exceeded, partial discharge processes can occur. The corresponding voltage is called partial discharge inception voltage (PDIV). These processes usually occur inside air-filled voids between insulation surfaces and lead to a rapid aging of the insulation material causing premature failure of the electric drive [4]. To avoid the occurrence of partial discharges, the insulation system has to be designed properly. This includes the prediction of the maximum voltage between neighboring conductors and between conductors and stator iron, respectively. The electric field also depends on the insulation material, more precisely on the permittivity. Regarding an arrangement of two adjacent insulated wires, a higher permittivity of the insulation material leads to a higher electric field in the air section between the wires. Therefore, a high value of the permittivity increases the risk of partial discharge inception. The exact value of the insulation material is often unknown or only determined for one certain frequency [5].

In inverter-driven electrical machines, voltage pulses with a high slew rate cause transient voltages exciting frequencies up to the Megahertz-range [6]. Additionally, the voltage at the machine's terminals can be subject to a high overshoot of up to two times the dc-link voltage [4]. To ensure a proper design of the insulation system and to predict the electric stress adequately, the voltage distribution along the winding has to be determined as well as the permittivity. For calculation of the transient voltages, different approaches [6], [7] can be used. However, for the permittivity, the characterization is not yet described sufficiently in literature. Therefore, in this work, an approach for the characterization of the relative permittivity at fast-rising voltage impulses is developed. In the first step, the frequency dependence of different insulation materials is measured using an impedance analyzer. After that, the relative permittivity is calculated based on voltage and current measurements at steep voltage slopes. Thereby it is possible to determine the transient electric stress around the peak voltage where usually the probability of partial discharge occurrence at its maximum [8], [9].

II. Technical Background

In this section, the technical background is discussed. First, the influence of the relative permittivity of the insulation material on the electric field is discussed. As partial discharge can occur in the air section between two wires, the arrangement of two adjacent enameled wires is considered. Subsequently, partial discharge processes are explained.

A. Permittivity

The influence of the relative permittivity of the insulation material can be schematically illustrated by the example of a plane capacitor. As depicted in Fig. 1, the dielectric interface between the two wires consists of two insulation layers and the air section. Usually, the insulation system of an electrical

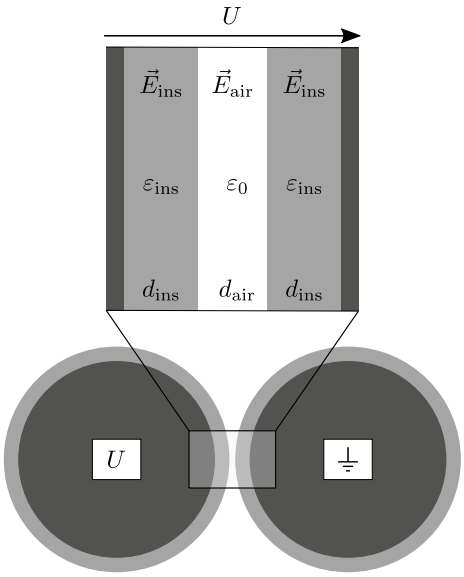

Fig. 1. Simplified plane capacitor [5].

machine is finished with impregnation or potting to reduce air inclusions. However, regardless of the process, air inclusions can never be completely avoided. This arrangement can therefore be seen as a worst-case assumption.

The voltage U can be described as follows:

$$U = E_{\mathrm{ins}} \cdot d_{\mathrm{ins}} + E_{\mathrm{air}} \cdot d_{\mathrm{air}} + E_{\mathrm{ins}} \cdot d_{\mathrm{ins}}. \tag{1}$$

Additionally, the boundary condition for the electric flux Density D is used (2). Using these equations, the influence of the insulation material on the electric field in air E_{air} can be expressed (3):

$$D = \text{const.} \Rightarrow \varepsilon_{\mathrm{r,ins}} \cdot \varepsilon_0 \cdot E_{\mathrm{ins}} = \varepsilon_0 \cdot E_{\mathrm{air}}, \tag{2}$$

$$E_{\mathrm{air}} = \frac{U}{2 \cdot d_{\mathrm{ins}} \cdot \dfrac{1}{\varepsilon_{\mathrm{r,ins}}} + d_{\mathrm{air}}}. \tag{3}$$

The electric field in air increases with increasing relative permittivity of the insulation material $\varepsilon_{\mathrm{r,ins}}$. From this connection, it can also be deduced that the occurrence of partial discharges is favored by a high relative permittivity.

B. Partial Discharge Processes

Partial discharge processes are gas discharge processes only bridging a part of the insulation. These processes can be described by the *Townsend* criterion. To cause a partial discharge, the local electric breakdown field has to be exceeded and a starting electron has to be available. Regarding a simplified arrangement with two electrodes, the starting electron is accelerated by the electric field from the cathode to the anode and collides with gas molecules. If the electron has sufficient kinetic energy, gas molecules are ionized meaning that at least one electron is released. This results in an avalanche-like increase of electrons in the direction of the anode. At the same time, the positively charged ions are moving in the opposite direction colliding with the cathode. These collision processes can lead to detrapping of electrons from the cathode providing new starting electrons. If at least one subsequent avalanche is triggered, the ignition condition according to *Townsend* is fulfilled [10]. The mathematical representation of these processes is given by:

$$\gamma \cdot \left[\exp\left(\int_{x=0}^{d} \alpha_{\mathrm{eff}} \left(E(x) \right) \cdot \mathrm{d}x \right) - 1 \right] \geq 1. \tag{4}$$

In this equation, γ describes the cathode reaction, i.e. how many electrons are released from the cathode per impacting ion. Besides, other effects like photo or field emission are covered by this parameter. The distance of the electrodes is indicated as d. The effective ionization coefficient α_{eff} depends on the local electric field and specifies the number of new electrons generated per unit length [10].

III. Measurements of the Permittivity

The relative permittivity is measured on round enameled wires. The insulation surface is coated with silver varnish over a length of $10\,\mathrm{cm}$ and forms the outer electrode of a cylindrical capacitor. The inner electrode is the copper conductor itself. First, the capacity is measured for a frequencies up to the Megahertz-range on five specimens. Subsequently, the relative permittivity is calculated by knowing the copper conductor radius and the insulation thickness. The material data are determined by using the approach presented in [5] and listed in Table I. After that, the capacity is measured at steep voltages slopes to analyze the influence of the voltage amplitude and overshoot behavior on the relative permittivity. The wires are named according to the insulation materials. It has to be noted that for a two-layer insulation only a combined relative permittivity can be determined with this approach.

TABLE I. Data of the examined wires.

Insulation layer 1	**Insulation layer 2**	**Copper diameter**	**Insulation thickness**
polyester-imid (PESI)	polyamide-imide (PAI)	$1.0\,\mathrm{mm}$	$40.2\,\mu\mathrm{m}$
corona-resistant PAI (CR-PAI)	-	$1.0\,\mathrm{mm}$	$35.2\,\mu\mathrm{m}$
polyether ether ketone (PEEK)	-	$1.15\,\mathrm{mm}$	$73.9\,\mu\mathrm{m}$

A. Influence of Frequency

To determine the frequency dependence of the permittivity, the capacity of the insulation is measured by using an impedance analyzer (Keysight E4990A) in a frequency

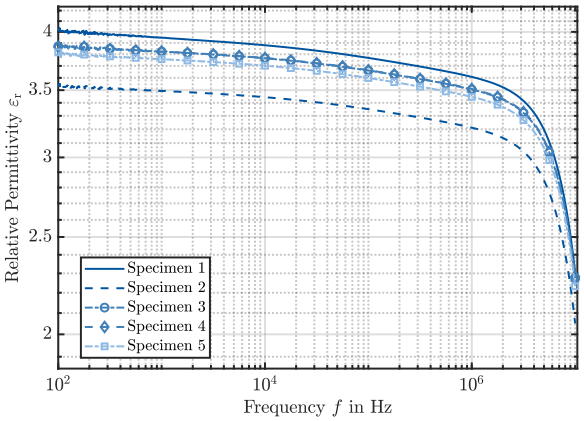

Fig. 2. Permittivity of the PESI-PAI wire.

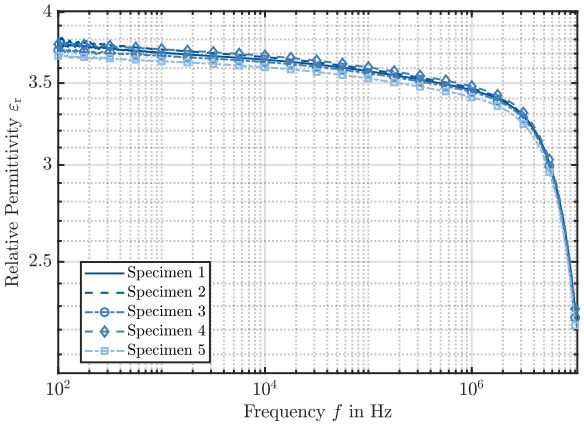

Fig. 3. Permittivity of the CR-PAI wire.

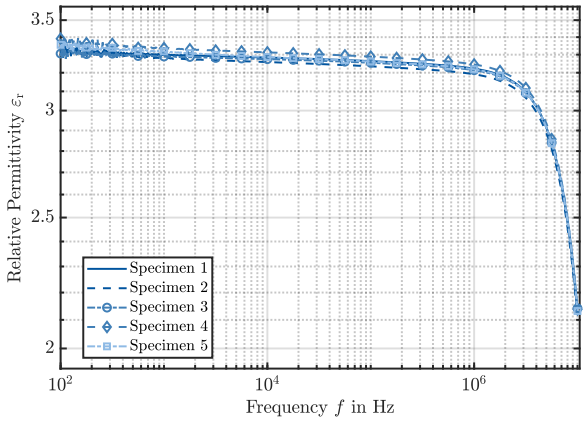

Fig. 4. Permittivity of the PEEK wire.

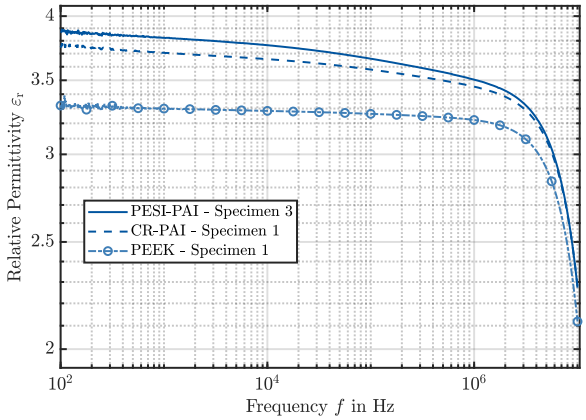

Fig. 5. Comparison of the frequency dependence of the different wires.

range from 100 Hz to 10 MHz. By knowing the geometry, in particular the copper radius R_1, the radius R_2 including the copper radius and the insulation thickness and the length of the electrodes l, the relative permittivity ε_r can be calculated using (5).

$$\varepsilon_r = C \cdot \frac{\ln(R_2/R_1)}{2 \cdot \pi \cdot \varepsilon_0 \cdot l}. \tag{5}$$

The results of the relative permittivity for the three different types of wires are shown in Fig. 2, Fig. 3 and Fig. 4. For the PESI-PAI wire, the relative permittivity at 100 Hz is between 3.54 and 4.01. The relative permittivity decreases with increasing frequency. Until a frequency of approximately 2 MHz, the median value of 3.86 decreases by 11 % to 3.43. At higher frequencies, the curve bends sharply corresponding to a large drop of the relative permittivity to a value of 2.3 at 10 MHz. A strong scattering of the measurement results can be observed, which allows conclusions to be drawn about manufacturing deviations with regard to the insulation layer thickness.

The measurement results of the CR-PAI wire show a significantly lower scattering. At 100 Hz, the relative permittivity is between 3.68 and 3.81. At 2 MHz, the median value is decreased by 10 % to 3.38. At higher frequencies, the same curve characteristics can be observed. The median value of the relative permittivity decreases to a value of 2.25.

The relative permittivity of the PEEK-layer at 100 Hz is between 3.31 and 3.39. The median value decreases by 5 % from 3.33 to 3.17 until 2 MHz. At 10 MHz, the median value is 2.13.

To compare the three different types of wires, the specimens with the median results are shown in Fig. 5. It can be seen that the PESI-PAI and CR-PAI wires exhibit a stronger frequency dependence than the PEEK wire.

B. Influence of Switched Voltages

To study the influence of impulse voltage on the permittivity, the specimen is connected to the output voltage of an SiC-module providing a bipolar voltage waveform. The SiC-module is supplied by a dc voltage source. The voltage across the insulation layer is measured using TEKTRONIX P5210A high-voltage differential probes. The current measurement is

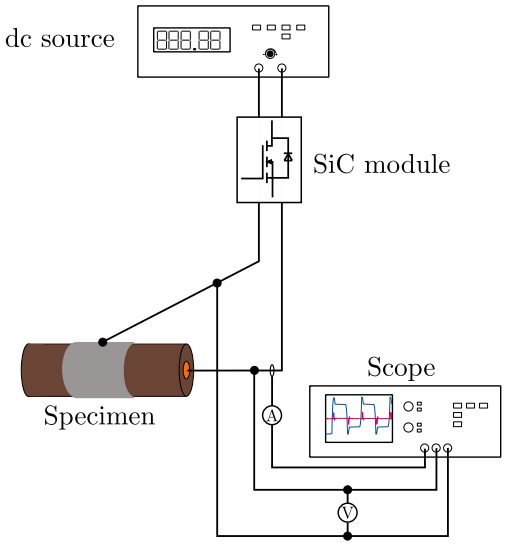

Fig. 6. Measurement setup at switched voltages.

performed with a TEKTRONIX TCP0030A current probe. The measurement setup is shown in Fig. 6. From the measurement results of voltage and current, the capacity of the arrangement can be calculated using (6):

$$i_\mathrm{c} = C \cdot \frac{\mathrm{d}u}{\mathrm{d}t}. \tag{6}$$

The relative permittivity in time domain is calculated by using (5). It has to be noted, that the validity of the results is limited to the section in which a change of the voltage $\mathrm{d}u/\mathrm{d}t$ and a measurable current occur. In the following, reference is made to two quantities: the maximum relative permittivity during the voltage overshoot $\varepsilon_{\mathrm{r,max}}$ and the relative permittivity $\varepsilon_{\mathrm{r,pk}}$ at the peak voltage U_pk. To predict the maximum stress on the insulation, the relative permittivity $\varepsilon_{\mathrm{r,pk}}$ at the peak voltage is assumed to be the relevant quantity.

The relative permittivity is studied for five different values of the dc-link voltage. The voltage has a high overshoot with a slew rate of up to $32\,\mathrm{kV\,\mu s^{-1}}$ and an oscillation frequency of 8 MHz to 11 MHz depending on the type of wire and dc-link voltage. The switching frequency used varied from 10 kHz to 50 kHz.

For a switching frequency of 10 kHz, the results are presented in Fig. 8. From the course of the relative permittivity, no distinct dependence on the dc-link voltage is discernible. The only remarkable fact is that at 100 V the relative permittivity $\varepsilon_{\mathrm{r,pk}}$ is comparatively low, particularly for the PESI-PAI and CR-PAI wire. In the studied voltage range, the maximum values for $\varepsilon_{\mathrm{r,pk}}$ are: 4.02 (PESI-PAI), 3.65 (CR-PAI) and 3.71 (PEEK). The values for the maximum relative permittivity $\varepsilon_{\mathrm{r,max}}$ are on average 8 % higher.

The dependence on the switching frequency f_sw is exemplary shown for specimen 3 of the PESI-PAI wire in Fig. 9. For most dc-link voltages, the relative permittivity $\varepsilon_{\mathrm{r,max}}$ is highest at the lowest switching frequency and lowest at the highest switching frequency. This coincides with the results of the first conducted study on the frequency dependence.

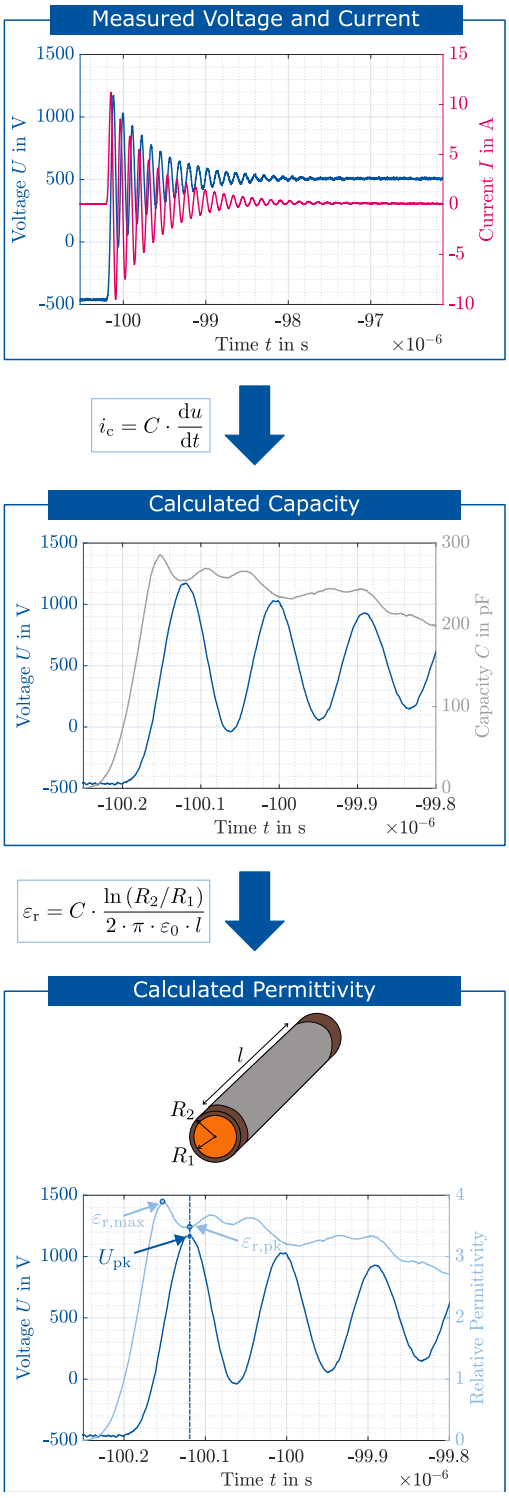

Fig. 7. Calculation of the relative permittivity.

C. Discussion of the Results

In Fig. 10, four different results are compared:

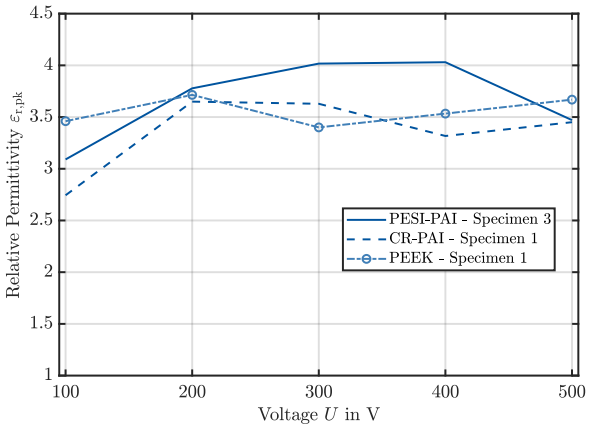

Fig. 8. Comparison of the relative permittivity at peak voltage.

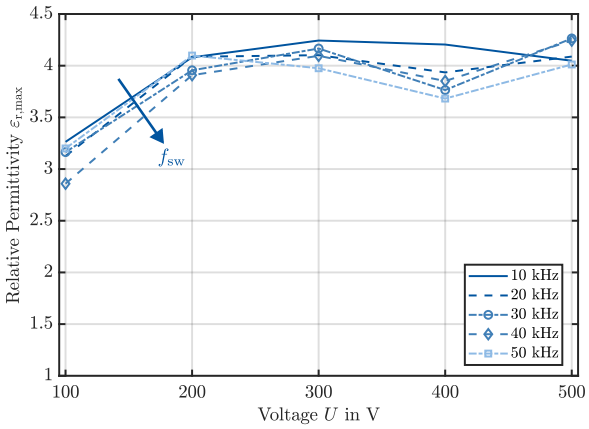

Fig. 9. Comparison of the relative permittivity at peak voltage.

- the relative permittivity ε_r at 100 Hz measured with the impedance analyzer,
- the relative permittivity ε_r at 10 kHz corresponding to the switching frequency of the impulse voltage,
- the relative permittivity $\varepsilon_{r,pk}$ at the peak value of the impulse voltage and
- the relative permittivity $\varepsilon_{r,max}$ at the impulse voltage.

In the design process, the maximum electric stress has to be evaluated. At a switching frequency of 10 kHz, the highest values of the relative permittivity are measured. When comparing the results, it becomes clear that the value of the relative permittivity is underestimated if only the results of the impedance analyzer are used, particularly for the PESI-PAI and PEEK wire. For these two wires, the relative permittivity at peak value of the impulse voltage is 7 % and 13 % higher, respectively. From the results of Fig. 8 it is assumed that the relative permittivity of the insulation material significantly depends on the electric field.

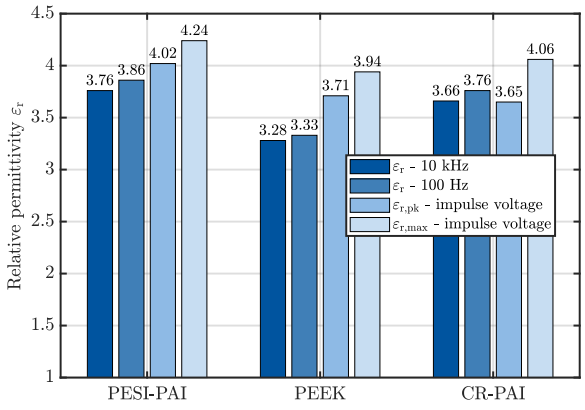

Fig. 10. Comparison of the relative permittivity.

IV. Electric Stress in Low-Voltage Electrical Machines

In this section, the electric stress in low-voltage electrical machines is discussed. Firstly, the propagation of voltage waves along the winding is explained followed by a case study of the estimation of the maximum electric stress of an exemplary application. To determine the PDIV for the turn-to-turn insulation, a two-dimensional finite-element-based simulation model is set up. This model is fed by the permittivity values determined in this paper. The simulation results are used to calculate the maximum dc-link voltage for the application.

A. Voltage Wave Propagation

In applications with wide-bandgap semiconductors, a high overshoot voltage can occur at the terminals of the machine. The overshoot depends on different factors like cable length, voltage rise time and impedance of the machine. The overshoot behavior is more pronounced, the longer the cable is and the faster the voltage rise is. The overshoot factor is defined as follows:

$$OF = \frac{U_{pk}}{U_{dc}}. \tag{7}$$

The peak voltage is denoted as U_{pk}, the dc-link voltage as U_{dc}. Under adverse circumstances, the peak voltage can reach two times the dc-link voltage [4]. The incoming voltage wave propagates along the winding with a finite propagation velocity of approximately 50 % of light speed [6]. The voltage rise time of modern inverters can be lower than 50 ns. Within this period of time, the voltage wave travels 7.5 m, which is generally much less than the length of the winding. Consequently, high electric potential differences are expected between adjacent wires. A schematic cross-section of a stator slot with an exemplary potential distribution is depicted in Fig. 11. The electric potential corresponds to the turn number inside the winding. In this arrangement, the first and the last turn of the winding are adjacent. This can be seen as the worst-case scenario meaning that the turn-to-turn insulation is stressed by

the maximum potential difference. Regarding the turn-to-turn insulation, the insulation layer of one wire is stressed by up to $50\,\%$ of the test voltage U, if the distance of the wires is minimized.

B. Maximum Electric Stress of Turn-to-Turn Insulation

The maximum electric stress is calculated according to the qualification tests specified in IEC 60034-18-41 [11]. From the specifications, a test voltage $U_{\mathrm{test,pk/pk}}$ is determined. The insulation system has to withstand this voltage without the occurrence of a partial discharge. The dc-link voltage U_{dc} is multiplied by various safety factors. For the turn-to-turn insulation, the following formula is used:

$$U_{\mathrm{test,pk/pk}} = 2 \cdot a \cdot 0.7 \cdot U_{\mathrm{dc}} \cdot OF \cdot NF \cdot PD \cdot TF. \quad (8)$$

Based on the fact that the turn-to-turn insulation can face both the positive and negative voltage edge, a factor of 2 is considered. The factor a indicates the percentage of the voltage, which is maximum between to adjacent wires. For a fast-rising voltage with a rise time of $50\,\mathrm{ns}$, a is equal to 0.9. For a rise time below, it tends towards 1. To consider a potential shift of the zero-point of the inverter, a factor of 0.7 is introduced. In addition to the overshoot factor OF, the factor NF is used to consider an increase of the supply voltage during operation. Furthermore, a safety factor PD with a value of 1.25 is applied as well as the temperature factor TF considering the temperature increase and thus a reduced PDIV during operation. For an operation temperature equal to or higher than $155\,^{\circ}\mathrm{C}$, a maximum value of 1.3 is prescribed. A more detailed discussion of the derivation of the test voltage can be found in [12].

C. Case Study

The following is a case study of an electric drive train. Two different configurations are considered. For the first example (A), the parameters of the voltage correspond to the parameters of the bipolar voltage used for characterization of the relative permittivity in this paper. An overshoot factor of 2 is calculated and a switching frequency of $10\,\mathrm{kHz}$ is used. The voltage rise time is $50\,\mathrm{ns}$. The second example (B) describes an application with a reduced overshoot factor of 1.2 corresponding to a very short connection cable between inverter and electric machine. The values for both examples are summarized in Table II.

TABLE II. Safety Factors for Calculation of the Test Voltage.

Factor	Value (A)	Value (B)
a	0.9	0.9
OF	2	1.2
NF	1.1	1.1
PD	1.25	1.25
TF	1.3	1.3

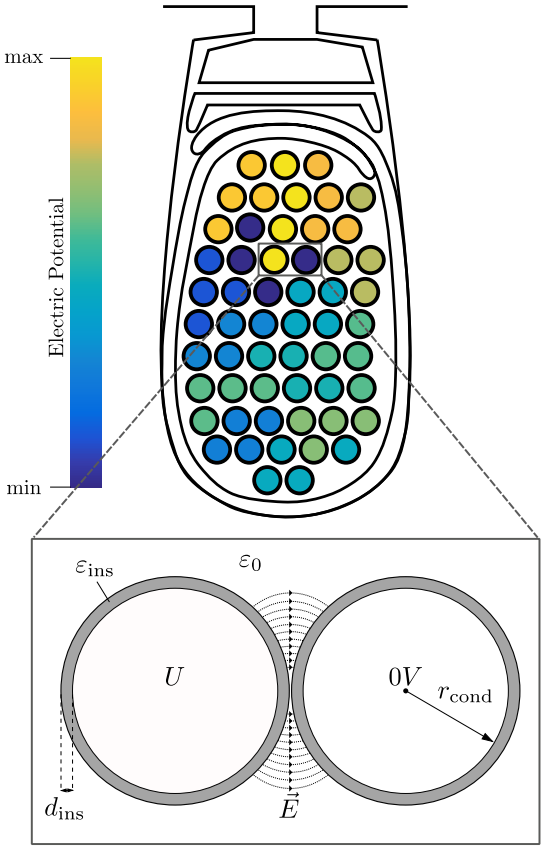

Fig. 11. Distribution of the electric potential and simulation model.

For example A with a high overshoot factor, the dc-link voltage is overall multiplied by 4.5, for a overshoot factor of 1.2 with 2.7 to calculate the test voltage.

D. Simulation Model

To calculate the PDIV according to the *Townsend* criterion, a two-dimensional finite-element model is set up. In addition to the test voltage U, the copper radius of the wire r_{cond}, the insulation thickness d_{ins} and the permittivity $\varepsilon_{\mathrm{ins}}$ are input parameters of the model. For numerical reasons, a distance of $2\,\mu\mathrm{m}$ is introduced between the wires. The setup of the model is also shown in Fig. 11 including exemplary electric field lines in the air section.

The PDIV is calculated for all three wires for the specimen with the median results using the measured parameter $\varepsilon_{\mathrm{r,pk}}$ at $10\,\mathrm{kHz}$. The coefficient γ was already determined in [5]. This parameter and the simulation results are listed in Table III. The other data are listed in Table I. To calculate the PDIV, the electric field distribution is first calculated. After that, a model of the electric field lines in air is set up. The field lines are sampled along their length in discrete steps. The local effective ionization coefficient is calculated according to [13]. The test voltage U is varied until the ignition condition (4) is fulfilled for one field line. The corresponding voltage is taken as the peak value for the PDIV.

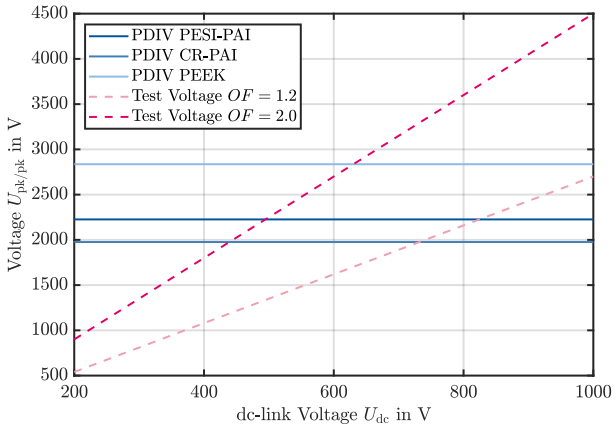

Fig. 12. Comparison of the results.

TABLE III. Simulation Parameters and Results.

Wire	γ	$\varepsilon_{\mathrm{r,ins}}$	**PDIV (pk)**	**PDIV (pk/pk)**
PESI-PAI	$0.478{\cdot}10^{-}3$	3.76	1113 V	2226 V
CR-PAI	$1.1 \cdot 10^{-}3$	3.66	988 V	1976 V
PEEK	$0.559{\cdot}10^{-}3$	3.71	1418 V	2836 V

E. Discussion

In the following, the suitability of the different wires is discussed. A comparison of the simulated PDIV values of the wires and the test voltage $U_{\mathrm{test,pk/pk}}$ is depicted in Fig. 12. The PESI-PAI wire is suitable for up to a dc-link voltage of 495 V for an overshoot factor of 2 and 824 V for $OF = 1.2$. The PDIV of the CR-PAI wire is significantly lower than that of the PESI-PAI wire because of a thinner insulation layer and a higher value of γ, although the permittivity is slightly lower. Therefore, the dc-link voltage is limited to 440 V and 732 V, respectively. Due to a comparatively thick insulating layer, the PDIV of the PEEK wire is the highest, leading to a larger range of possible values for the dc-link voltage. The calculated values are 630 V for the considered large overshoot and 1030 V for the lower overshoot.

V. Conclusions

In this paper, the relative permittivity of round wires is characterized in a frequency range from 100 Hz to 100 MHz with an impedance analyzer. Additionally, an approach for the characterization at impulse voltages with a high overshoot is presented for different switching frequencies. It has to be noted that this approach is only applicable for round wires. For rectangular wires used in hairpin windings, the capacity can be measured with a similar setup but the relative permittivity has to be calculated using an finite-element-based approach since the insulation layer thickness is usually not homogeneous due to effects such as thinning of the edges.

The comparison of the measurement results shows that the frequency-based measurement leads to an underestimation of the electric stress as the relative permittivity also depends on the electric field. The highest values occur at a switching frequency of 10 kHz, as expected. For the PESI-PAI and PEEK wire, the relative permittivity is 7 % and 13 % higher than the value measured with the impedance analyzer.

Additionally, a case study is performed for considering an electric drive train with different values for the overshoot factor. To calculate the PDIV of the wires, a simulation model is set up with the material data and the test voltage as input parameters. Subsequently, the electric field in the air between the wires is calculated. Inside the air section, the gas discharge process is modeled using the ignition condition described by *Townsend*. The results of the simulation are compared to the test voltage the wires must withstand. This allows evaluating the suitability of the different wires for various values of the dc-link voltage.

References

[1] C. Jung, "Power up with 800-V systems: The benefits of upgrading voltage power for battery-electric passenger vehicles," *IEEE Electrification Magazine*, vol. 5, pp. 53–58, 2017.

[2] B. Wrzecionko, J. Biela, and J. W. Kolar, "Sic power semiconductors in hevs: Influence of junction temperature on power density, chip utilization and efficiency," in *2009 35th Annual Conference of IEEE Industrial Electronics*, 2009, pp. 3834–3841.

[3] B. Florkowska, P. Zydron, and M. Florkowski, "Effects of inverter pulses on the electrical insulation system of motors," in *2011 IEEE International Symposium on Industrial Electronics*, 2011, pp. 573–578.

[4] M. Kaufhold, H. Aninger, M. Berth, J. Speck, and M. Eberhardt, "Electrical stress and failure mechanism of the winding insulation in pwm-inverter-fed low-voltage induction motors," *IEEE Transactions on Industrial Electronics*, vol. 47, no. 2, pp. 396–402, 2000.

[5] N. Driendl, F. Pauli, and K. Hameyer, "Characterization of insulation material parameters in low-voltage electrical machines," in *2022 International Conference on Electrical Machines (ICEM)*, 2022, pp. 1314–1320.

[6] F. Pauli, N. Driendl, S. Mönninghoff, and K. Hameyer, "Comparison of concentrated winding topologies considering transient voltages in the winding system of inverter-driven low-voltage machines," *Archives of Electrical Engineering*, vol. vol. 71, no. No 4, pp. 865–880, 2022.

[7] O. Magdun, S. Blatt, and A. Binder, "Calculation of stator winding parameters to predict the voltage distributions in inverter fed ac machines," in *2013 9th IEEE International Symposium on Diagnostics for Electric Machines, Power Electronics and Drives (SDEMPED)*, 2013, pp. 447–453.

[8] N. Driendl, F. Pauli, and K. Hameyer, "Modeling of partial discharge processes in winding insulation of low-voltage electrical machines supplied by high $\mathrm{du/dt}$ inverters," in *IECON 2019 - 45th Annual Conference of the IEEE Industrial Electronics Society*, vol. 1, 2019, pp. 7102–7107.

[9] P. McLaren and M. Abdel-Rahman, "Modeling of large ac motor coils for steep-fronted surge studies," *IEEE Transactions on Industry Applications*, vol. 24, no. 3, pp. 422–426, 1988.

[10] A. Küchler, *High Voltage Engineering: Fundamentals - Technology - Applications*, ser. VDI book. Springer Berlin Heidelberg, 2017.

[11] *Rotating electrical machines - Part 18-41: Partial discharge free electrical insulation systems (Type I) used in rotating electrical machines fed from voltage converters – Qualification and quality control tests*, IEC Standard 60 034-18-41 ed. I, November 2014.

[12] N. Driendl, F. Pauli, and K. Hameyer, "Influence of ambient conditions on the qualification tests of the interturn insulation in low-voltage electrical machines," *IEEE Transactions on Industrial Electronics*, vol. 69, no. 8, pp. 7807–7816, 2022.

[13] R. Morrow and J. J. Lowke, "Streamer propagation in air," *Journal of Physics D: Applied Physics*, vol. 30, no. 4, pp. 614–627, 1997.